Design and modelling of a novel compact power cycle for low temperature heat sources

Wronski, Jorrit; Skovrup, Morten Juel; Elmegaard, Brian; Rislå, Harald Nes; Haglind, Fredrik

Published in:
Proceedings of ECOS 2012

Publication date:
2012

Document Version
Publisher's PDF, also known as Version of record

Design and Modelling of a Novel Compact Power Cycle for Low Temperature Heat Sources

Jorrit Wronski[a], Morten Juel Skovrup[b], Brian Elmegaard[c], Harald Nes Rislå[d] and Fredrik Haglind[e]

[a] *Technical University of Denmark, Kgs. Lyngby, Denmark, jowr@mek.dtu.dk,* ***CA,***

[b] *IPU, Kgs. Lyngby, Denmark, mjs@ipu.dk,*

[c] *Technical University of Denmark, Kgs. Lyngby, Denmark, be@mek.dtu.dk,*
[d] *Viking Heat Engines, Kristiansand, Norway, hnr@vdg.no,*

[e] *Technical University of Denmark, Kgs. Lyngby, Denmark, frh@mek.dtu.dk*

Abstract:

Power cycles for the efficient use of low temperature heat sources experience increasing attention. This paper describes an alternative cycle design that offers potential advantages in terms of heat source exploitation. A concept for a reciprocating expander is presented that performs both, work extraction and heat addition. Heated by thermal oil, evaporation takes place in two expansion chambers with a transfer of the working fluid at an intermediate pressure level. Using saturated liquid as feed leads to an expansion in the two-phase domain. A dynamic model of this expander is used to determine the state of the working fluid during the process. Based on this model, a first optimisation by means of changed valve timing is conducted and the results of this scenario are shown in this paper. The heat transfer during expansion is investigated and used to establish a representation of the dynamic calculation results for use with a steady state cycle evaluation. An organic Rankine cycle model is developed and used for a comparison. The performance of the expander itself and the different requirements regarding heat source and temperature levels are studied.

Keywords:

Alternative power cycle, two-phase expansion, reciprocating expander, organic Rankine cycle, waste heat recovery, low temperature heat sources.

1. Motivation and background

The world-wide energy demand increases constantly leading to an accelerated consumption of fossil fuels [1]. Rising prices for resources and fuels as well as the political atmosphere abet efforts in energy efficiency and the exploitation of renewable energy sources. Power cycles that convert low-grade heat to valuable electricity can help with both targets mentioned above. The energy efficiency of existing systems can be improved by utilising waste heat streams and several renewable heat supplies like biomass boilers, solar thermal collectors and geothermal sources that meet the requirements of such a cycle.

Organic Rankine cycles (ORC) gain an increasing amount of attention from the scientific and the business community. Plants are being erected and ongoing optimisation efforts increase performance and reliability. However, there is no established solution in the capacity range below 25 kW of electrical output. To circumvent the obstacles faced by turbo machinery at these low capacities, research has turned towards volumetric expanders. There are ongoing efforts to assess the feasibility of for example scroll [2], screw [3] and vane [4] type expansion devices for low capacity applications. By investigating a reciprocating expander, this study contributes information on an additional design.

The proposed cycle was initially sketched by Viking Heat Engines (VHE) and is based on the idea to combine isothermal heat addition and expansion. Excluding evaporation from the primary heat exchanger abets an efficient heat supply while employing compact components. Furthermore, the

system should not rely on a regenerator for efficient operation and offer economic advantages by using a large share of parts from the automotive sector. Pursuing the idea to design a compact power cycle containing a reciprocating expander, a first prototype was designed and set to operation by IPU in a shared workshop located at the Technical University of Denmark (DTU).

To assist with the further optimisation of the prototype, a dynamic model is built that incorporates key features of the existing mechanical design. This model connects two infinitely large reservoirs of design point feed pressure and condensing pressure. The existing prototype has not been operated at these conditions. Yet the characteristics of the simulated pressure curves match with the measured data during operation at lower pressures. This paper introduces the new power cycle and illustrates the concept by presenting first simulation results. In a next step, a steady state representation is developed. Including the expander in a power cycle enables the comparison to a Rankine process with the same fluid and similar operating conditions highlighting differences and similarities of the two power cycles.

2. Design

2.1. Boundary conditions and system layout

The test rig for the experiments, to which this modelling study relates, consists of the classical power cycle components. Condensed working fluid, state 1, coming from a water-cooled plate-type counterflow condenser passes a pump, state 2, and enters the primary heat exchanger. In this second counterflow plate-type device, the pressurised liquid is heated by thermal oil to state 3. It enters the expansion device and is first throttled to state 4 and afterwards expanded to state 5, which corresponds to the condenser inlet conditions. In addition to the basic components of a Rankine cycle, the expander is also connected to the heat supply and delivers thermal energy to the working fluid during the expansion. Figure 1 helps to illustrate the process and clarifies the order in which the working fluid passes the different components.

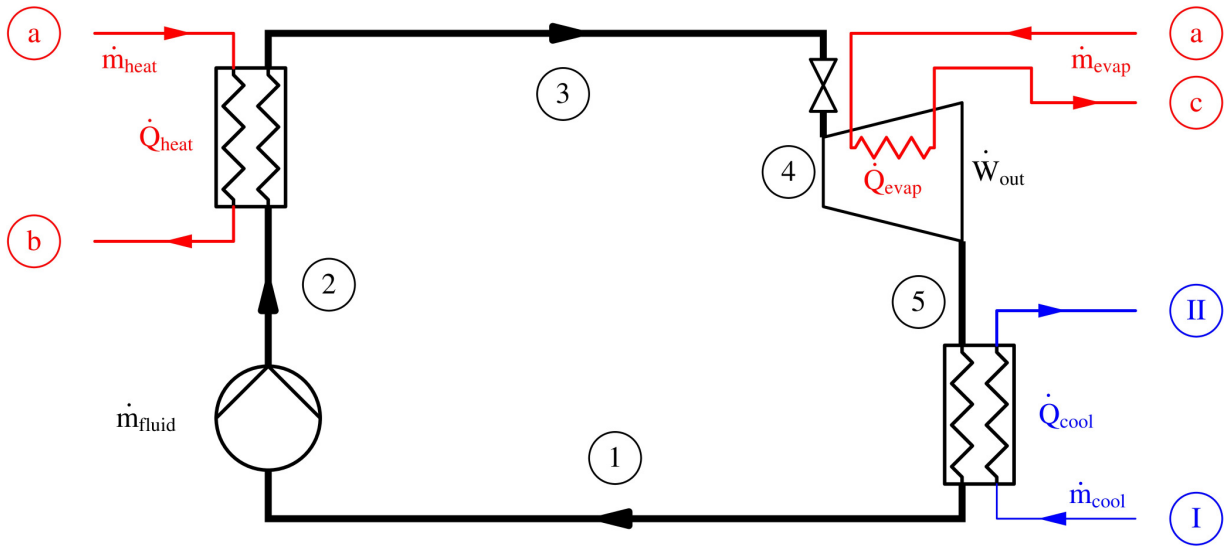

Fig. 1. Layout of the test facilities used in modelling and experiments.

The energy input to the presented heat-to-power conversion system is realised as a loop of thermal oil with a 400 l buffer tank, which is equipped with five temperature controlled electrical heaters giving a total capacity of 60 kW. Due to the large amount of oil and the limited operating time of the test facility, the hot oil is assumed to have a constant temperature of 200 °C. Heat is supplied to the primary heat exchanger and to the expander from the storage tank mentioned above, resulting in

similar inlet conditions, which are denoted with an “a” in Fig. 1. Employing pentane as working fluid enables the test facility to be built from standard components that are certified for pressures up to 35 bar while respecting the expected temperature levels in the components.

2.2. Expander design

Being part of ongoing experimental investigations by IPU and VHE, the calculations in this work are based on a design proposed by these companies. The current concept includes a double-acting piston expander that extracts work from a pressurised fluid by means of a two-stage expansion. The first stage, which is referred to as the high pressure expansion chamber (HPC), contains a built-in heat exchanger that is connected to the hot oil loop and utilises a fixed area for heat transfer to the working fluid during expansion. The same oil line also heats the walls of the low pressure expansion chamber (LPC) before it is fed back into the storage tank. The two stages are connected via a transfer line, which is controlled by a mechanically triggered valve. Injection and exhaust are activated shortly before the volume in HPC and LPC is smallest and largest, respectively. Being confined by the same piston, the bottom dead centre (BDC) for the first stage at 0° crank shaft angle θ coincides with the BDC of the second stage. Since the HPC is located below the piston, its volume is smallest at BDC and largest at top dead centre (TDC). The volume of the second stage changes in the opposite way.

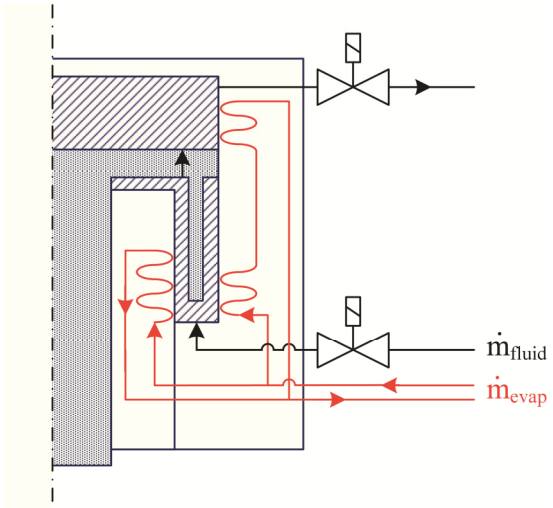

Fig. 2. Cross-sectional cut of the double-acting piston, shown as shaded parts, close to bottom dead centre with sketched heat exchangers, inlet and exhaust valves. Transfer lines and valves inside the piston and are omitted here for simplicity. The volume filled with working fluid is shown with a diagonal pattern.

The sketch of the expander, Fig. 2, illustrates the shape of the device described above. The working fluid enters from the bottom. After injection, it evaporates while receiving heat from the two heated walls of the HPC. Designing the lower chamber as a ring increases the wall area to volume ratio, which is beneficial for the heat exchange process. The additional ring mounted on the bottom side of the piston leads to a decrease in clearance volume and provides a further enhancement of the volume to wall area ratio. The transfer line opens as the piston reaches TDC and the second expansion stage takes place in the two connected volumes.

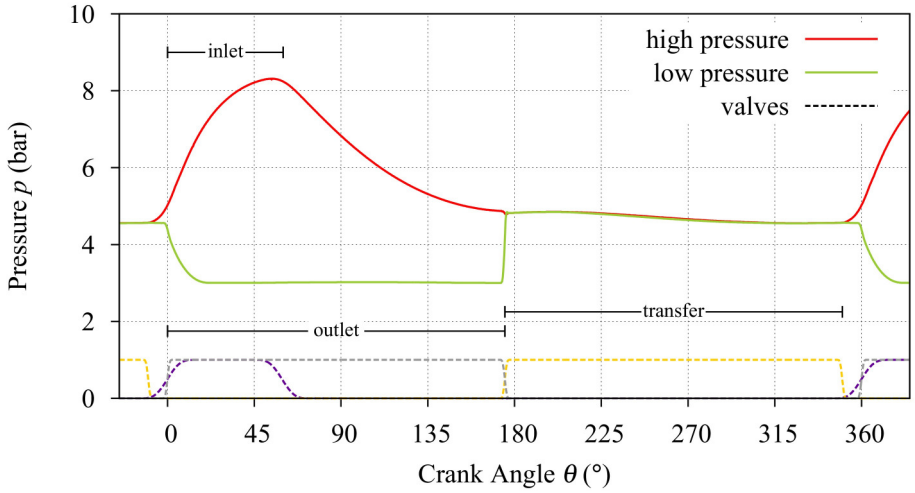

Fig. 3. Pressure in high and low pressure expansion stage, solid lines, and valve states, dashed lines, during one crank shaft revolution.

Following the pressure residing in both expansion volumes for one complete crank shaft rotation gives a good impression of how the two stages are connected and when work can be extracted from the fluid. The series of data shown in Fig. 3 was obtained from a preliminary test run of the model described below, a mixture of liquid and vapour in the supply line and pressures below the intended operating pressures. To clarify the control strategy of the device, the states of the valves for inlet, transfer and exhaust of the fluid are also given as curves alternating between 0 and 1 representing closed and open position, respectively. As mentioned above, high pressure working fluid is injected into the HPC at 0° θ compressing fluid in the clearance volume and elevating the chamber pressure to a maximum at approximately 55° θ. Simultaneously, the exit port of the LPC opens and fluid leaves this part of the device while the pressure becomes similar to the condenser conditions before an isobaric exhaust takes place. Approaching 180° θ, the exit line closes and both chambers get connected via the transfer ports resulting in an almost constant pressure while fluid gets transferred from first to second expansion stage. Due to larger footprint of the LPC, the overall confined volume increases during the transfer of fluid. Hence, the low pressure expansion takes place in both chambers despite the decreasing volume in the HPC. The increased piston surface in the LPC results in a force that successfully counteracts fluid friction in the transfer line.

3. Simulations

3.1. Dynamic expander model

In order to provide assistance regarding the experiments with the custom-built expander, a dynamic model is used to estimate performance and to provide insights in the possible behaviour of the machine. A thermodynamic simulation of the expander's operation was implemented with the software Engineering Equation Solver (EES) [5] using the built-in property functions for pentane originally presented in [6]. The mechanical system of expansion chamber, piston, connection rod, crank arm and crank shaft is considered to operate without friction, lubrication or any deformation. Furthermore, a constant rotational speed is assumed. Hence, only masses of reciprocating parts and the oscillating equivalents of rotating components have to be taken into account.

The basis of the simulation is formed by defining the rate of internally performed work as the product of pressure and instantaneous change in chamber volume

$$\dot{W} = -p \cdot \dot{V} . \qquad (1)$$

Other flows over the systems boundaries occur in terms of heat and mass transfer. The latter also contributes to the exchange of energy by means of enthalpy that enters and leaves the control

volume. The differential expression for internal energy can be used to combine the different influences. Integrating the equation

$$-\frac{dU}{dt} = \frac{dH}{dt} + \dot{Q} + \dot{W} \quad \text{with} \quad \frac{dH}{dt} = \dot{m}_{in} \cdot h_{in} + \dot{m}_{out} \cdot h_{out} \tag{2}$$

yields a way to follow the development of the state of the fluid inside the control volume.

In this work, a heavily idealised simulation is presented that is subject to several simplifications. Compressibility is neglected for the calculation of all flows and the specific mass flow per hydraulic area is expressed by

$$\dot{m}/A = c_d \sqrt{2 \cdot \Delta p \cdot \rho}\,. \tag{3}$$

In (3), Δp is the pressure difference between two connected volumes and ρ denotes the density of the upstream reservoir. The discharge coefficient c_d is always smaller than unity and calculates the pressure drop accounting for the losses in a valve. It is a measure of how much flow develops in comparison to ideal lossless conditions. A second way in which flow resistances are included in the calculations is the available area A. In case of valves, the maximum flow area A_0 is multiplied by a factor to obtain the effective area. This value is modified according to the opening state of the respective port. The switch from opened, 1, to closed, 0, and back is calculated by the function

$$\vartheta_A(\theta) = \frac{-3}{4}\left(\frac{1}{3}\cdot\cos^2\phi\cdot\sin\phi + \frac{2}{3}\sin\phi\right) + \frac{1}{2} \quad \text{with} \quad \phi = \frac{\theta - \theta_t}{\Delta\theta}\cdot\pi\,, \tag{4}$$

which was initially proposed by [7] and provides a sufficiently smooth transition. The second part of (4) relates the actual crank angle degree θ to the desired switching point θ_t and the length of the transition from one state to the other $\Delta\theta$. Employing different trigger angles and transition durations, (4) is used to generate the alternating functions shown on the bottom part of Fig. 3.

Another important assumption is related to the heat fluxes. It is assumed that heat is only released by the internal heat exchanger and the cylinder walls. Areas in contact with the fluid belonging to the piston and the rest of the housing do not participate in the heat exchange. Furthermore, this heat transfer is of an exclusively convective nature. Neither radiation nor conduction contributes to the energy exchange. Hence, the only equation describing the heat exchange in one chamber is

$$\dot{Q} = \alpha \cdot A_{wall} \cdot \left(T_{wall} - T_{fluid}\right). \tag{5}$$

In order to solve (5) for each of the chambers, the effective surface of heated walls and internal heat exchanger A_{wall} and the temperature difference have to be determined. The first is a function of the geometry only and the latter is the difference between the average fluid temperature and the fixed wall temperature of 180 °C. An additional simplification leads to a value for the heat transfer coefficient α, which is implemented as a function of the vapour content in the chambers.

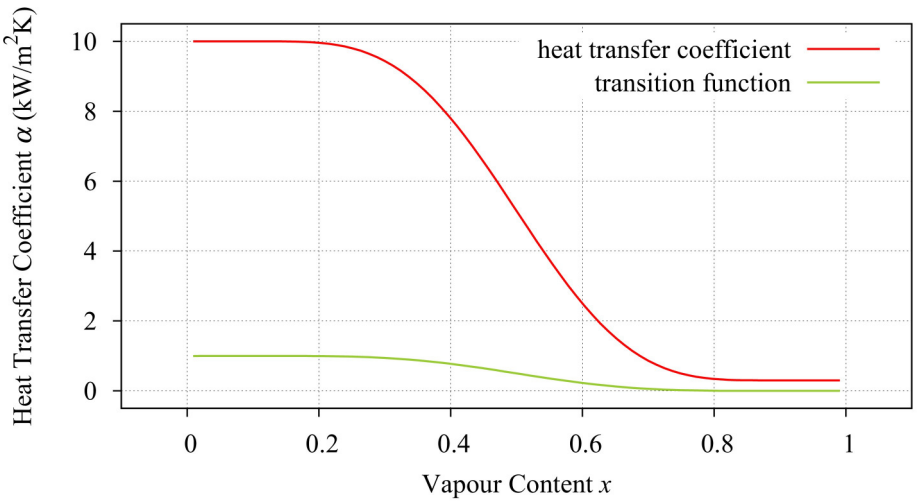

Fig. 4. Heat transfer coefficient as function of vapour content.

To model this variation of the heat transfer properties as shown in Fig. 4, an upper and a lower limit have to be defined. Depending on the superheat at the wall, [8] found that heat transfer coefficients of up to 10 kW/m^{2}K occur in boiling pentane for natural convection in a confined space. This value is used as the upper limit for α. Employing a lower limit of 0.3 kW/m^{2}K and the same general smooth transition equation from [7] as above yields

$$\vartheta_\alpha(x) = \frac{-3}{4}\left(\frac{1}{3}\cdot\cos^2\phi\cdot\sin\phi + \frac{2}{3}\sin\phi\right) + \frac{1}{2} \text{ with } \phi = \frac{x-0.5}{0.8}\cdot\pi\,, \qquad (6)$$

where the centre of the transition process is set to 0.5 and the interval length is defined as 0.8. Thus the heat transfer coefficient is defined as $\alpha/(\text{kW/m}^2\text{K}) = \vartheta_\alpha\cdot 10+(1-\vartheta_\alpha)\cdot 0.3$ and depends on the vapour content only. It decreases from 10 kW/m^{2}K for 10% gaseous fluid to the lower limit of 0.3 kW/m^{2}K at 90% vapour.

After defining all the necessary equations to simulate the expander operation, the actual calculation is carried out by means of an integration over crank shaft angle. When steady state operation is reached in the solution, similar results are obtained for every revolution of the crank shaft. To assure such stable conditions, one simulation run comprises at least six crank shaft revolutions and only the last two are used for further data analysis.

The model has been preliminarily validated by comparison to experimental data for the test operation described by Fig. 3. In contrast to these calculations, the simulations presented below were carried out with modified valve timing and design point feed conditions. Closing the exit ports before the end of the stroke leads to an increase of pressure and temperature. This common measure to optimise reciprocating expanders is also used in recent steam engine development [9]. Compressing the remaining fluid in the clearance volumes before admitting a new charge of working fluid minimises losses. The net power output decreases slightly, but there is a valuable gain in efficiency.

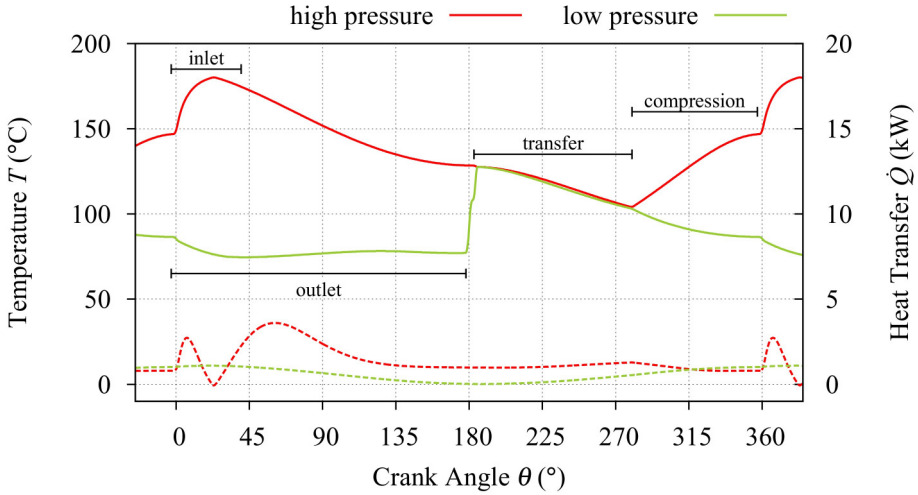

Fig. 5. Temperature, solid lines, and heat uptake, dashed lines, of both expansion chambers.

The temperature variation over crank angle is very much alike the pressure history. Therefore, the result of modifying the valve timing can also be seen on the temperature plot in Fig. 5. Again, admission of high pressure working fluid takes place around BDC at 0° θ. Saturated liquid in the feed line is throttled in the injection system and is sprayed onto the surface of the internal heat exchanger in the HPC. A high liquid fraction yields enhanced heat transfer, as described by (6), leading to an increased heat release from the walls. With progressing evaporation and expansion, temperature and pressure drop in the HPC. The effect of the precompression can be spotted as a two-step rise in temperature in the LPC around TDC at approximately 180° θ and similarly in the HPC during the last 80° θ of the revolution before BDC is reached again.

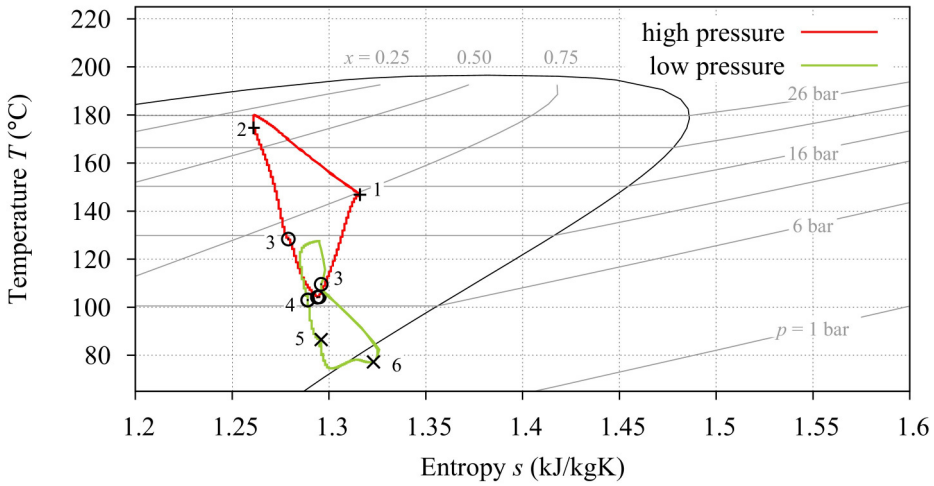

Fig. 6. Dynamic simulation of both expansion chambers, temperature over entropy for one crank shaft revolution.

Depicting the crank shaft revolution shown in Fig. 5 in terms of temperature and entropy, one obtains Fig. 6. The two cycles show the average state of the working fluid in both chambers and have to be read counter-clockwise. The BDC matches the right corner of the graph, 16 bar denote the end of the compression phase. The cross on the right hand side, point 1, is drawn at the opening angle of the inlet valve. During the following admission of working fluid pressure peaks at 26 bar while the average vapour content x in the chamber does not fall below 0.25. Evaporation and expansion start before the second cross, point 2, denotes the closure of the inlet. Reaching 11 bar, the chambers get connected and expansion takes place in the complete volume after an initial pressure increase in the LPC. Circles are drawn on both curves to illustrate the opening and closing of the transfer valves at point 3 and point 4, respectively. The states in the chambers are comparable when the transfer valves close. Both circles are next to each other at around 100 °C and the vapour content in the HPC is above 0.9. Afterwards, precompression elevates temperature and pressure in the high pressure part. Condensation occurs and eventually point 1 is reached. At the same time, expansion continues in the low pressure part of the machine. The two crosses on the graph for the LPC denote a state change of the exhaust valve to open, point 5, and back to closed, point 6. Hence, the final evaporation of the working fluids happens during exhaust and the precompression in the LPC takes place on the right hand side of the lower cycle between cross and circle, from point 6 to point 3 causing condensation of the working fluid.

3.2. Steady state expander model

This part of the paper describes the steady-state operation results based on the dynamic model presented above. By defining a simple and moderately accurate technique to account for the additional heat transfer during expansion, it is possible to compare the alternative expander to an ORC from a system perspective. The approach presented below is based on dividing the expansion into different steps with an isobaric intermediate heat addition.

To identify the temperatures and pressures at which the heat addition should take place, the heating calculated in the dynamic simulations is analysed with a greater level of detail. The average heat transfer rate during expansion $\dot{Q}_{evap}$ is 2 kW at a wall temperature of 180 °C. This number is sensitive to the chosen wall temperature and simulations with 160 °C and 220 °C yield 0.4 kW and 4 kW, respectively. Approximately three quarters of the heat are released in the high pressure chamber as Q_{HPC} and one quarter in the low pressure chamber as Q_{LPC},

$$Q_{LPC} = \frac{1}{4}\dot{Q}_{evap} \cdot \frac{60\ \mathrm{s/min}}{N} \text{ and } Q_{HPC} = \frac{3}{4}\dot{Q}_{evap} \cdot \frac{60\ \mathrm{s/min}}{N}. \qquad (7)$$

Looking for a steady state solution, the crank angle and time domain in Fig. 5 are neglected and the values for one crank shaft revolution are regarded as one set of data. In (7), the average heat transfer rate is divided by the rotational speed N of 1500 min^{-1} to obtain the amount of transferred heat per revolution. Combining the two remaining quantities temperature and heat transfer leads to the temperatures at which the actual heat addition takes place.

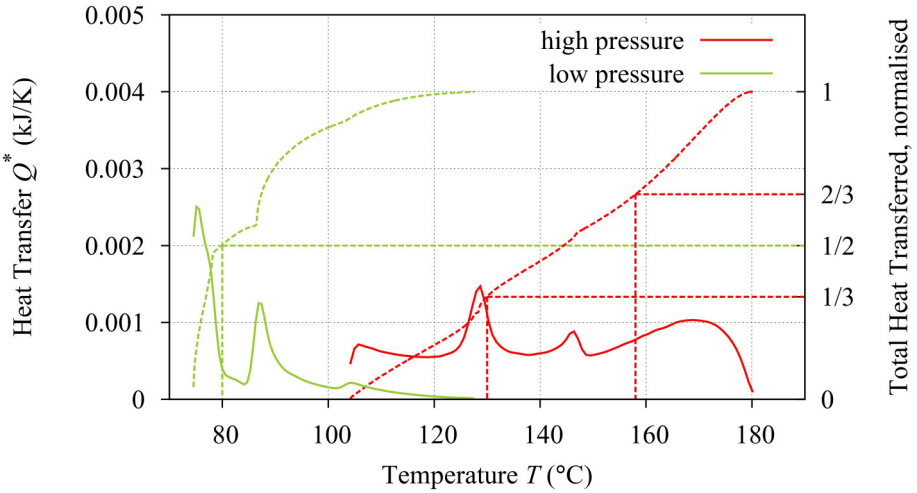

Fig. 7. Heat transfer, solid lines, and the normalised integrated heat transfer, dashed lines, during one crankshaft revolution mapped to bulk fluid temperatures.

The resulting Fig. 7 displays the same data as Fig. 5, but with the heat transfer plotted in relation to the bulk fluid temperature in both chambers. Q^* denotes the sum of all heat added during one crank shaft revolution at a certain temperature and is decoupled from crank angle and time domain. It can be seen that most heat is transferred to the LPC at lower temperatures. Whereas heat input to the HPC takes place in the range between 105 °C and 180 °C, which denote the beginning and the end of the curve for the HPC in Fig. 7. An integration of the heat transfer over temperature gives the total amount of added heat. To define suitable temperatures for the intermediate heating, one has to investigate the integral of the heat transfer per temperature, which is shown as dashed graphs in Fig. 7. For the LPC, all heat release is assumed to take place at the temperature at which the integrated heat transfer reaches half of its final value. Due to the large amount of heat entering the HPC, this heat transfer is split up into two portions that are applied at the temperatures corresponding to one third and two thirds of the integrated heat exchange. As depicted in Fig. 7, three temperatures are chosen for the intermediate heat transfer $T_{heat,3}$ 80 °C, $T_{heat,2}$ 130 °C and $T_{heat,1}$ 158 °C. Summarising the above, the heat uptake during expansion is split up as defined by

$$\frac{1}{2}Q_{LPC} = \int_{70\,^\circ\mathrm{C}}^{T_{heat,3}} Q^*_{LPC}dT; \frac{1}{3}Q_{HPC} = \int_{100\,^\circ\mathrm{C}}^{T_{heat,2}} Q^*_{HPC}dT; \frac{2}{3}Q_{HPC} = \int_{100\,^\circ\mathrm{C}}^{T_{heat,1}} Q^*_{HPC}dT. \qquad (8)$$

Hence, expansion is divided into four steps between which the amounts of heat given in (8) are added. Each step is considered adiabatic and assumed to have an isentropic efficiency $\eta_{is,exp}$ of 0.825. By defining these temperatures and efficiency, the extracted work matches with the results of the dynamic simulation and the same amount of heat is transferred during the expansion phase.

4. Comparison with an organic Rankine cycle

The presented two-phase expander can be operated in a setup similar to an organic Rankine cycle by adding heat in the preheater only. The same software, EES [5], is also used for the following calculations. For a comparison of the steady state operation, the auxiliary equipment is modelled in a similar manner. Both of the expanders are calculated as part of a comparable cycle consisting of condenser, pump and primary heat exchanger employing pentane as a working fluid. There are no temperature constraints regarding the heat utilisation. The oil loop may be cooled as much as

needed and the supply is of infinite capacity. However, the mass flow of thermal oil is constant and set to 0.15 kg/s for all considered systems. Furthermore, the condenser operates at a constant pressure of 3 bar and there is a subcooling of 1 K at the outlet. The feed pressure for the ORC is adjusted to 13 bar in order to obtain the highest possible power output at the given conditions. Expansion efficiency $\eta_{is,exp}$ is set to 0.825 for the ORC as well as for the adiabatic steps of the two-phase expansion. To account for the initial pressure losses calculated by the dynamic expander model, the feed pressure for the primary heat supply of the two-phase expansion at 30 bar is throttled isenthalpically to a maximum pressure of 25 bar. The ORC is equipped with a regenerator in addition to the two main heat exchangers before and after the pump, which operates with $\eta_{is,pump}$ of 0.5. All considered heat transfer takes place at isobaric conditions, without pressure loss, and with a fixed pinch point temperature difference ΔT of 10 K.

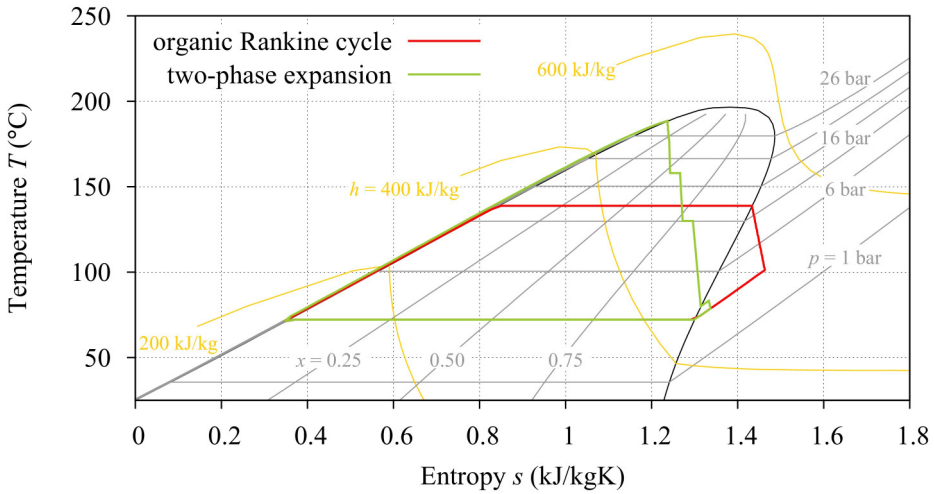

Fig. 8. Steady state simulation of two-phase expansion and organic Rankine cycle.

The resulting process is sketched in a temperature over entropy diagram in Fig. 8. This figure shows the effect of the multi-step expansion and the heat addition and illustrates the effect of the different feed pressures. The working fluid is only slightly superheated after the two-phase expansion process compared to the ORC expander outlet conditions. Defining the minimum temperature difference of 10 K determines the mass flows of working fluid and cooling media in evaporator and condenser as well as the amount of transferred heat in the regenerator. Heat input is modelled by a constant heat supply inlet temperature of 200 °C and a set of equations to approximate the properties of the heat transfer oil.

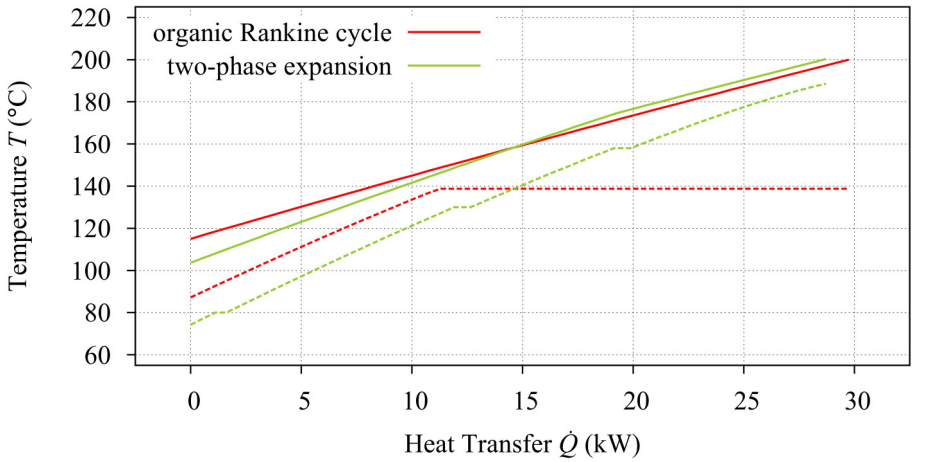

Fig. 9. Heat source, solid line, and working fluid, dashed line, during heat supply to both cycles.

Approximate experimental data provided by the supplier of the oil Texatherm HT22, AB&CO TT Boilers A/S, Greve, Denmark, was used to generate polynomials for the interdependency of heat capacity, density and temperature. On the cold side of the process, water is supplied at 30 °C and 3 bar. The corresponding fluid properties are calculated using equations by [10] and [11], which are already a part of EES. Due to the regeneration, the heat removal from the process looks similar in both configurations.

For the ORC, a working fluid flow of 0.076 kg/s is needed to obtain a suitable inclination of the line representing the heat receiver in Fig. 9 while respecting the defined minimum temperature difference at the given pressure. As a result, there is a large temperature difference of 60 K at the end of the heat transfer. The initial temperature of the working fluid is slightly higher in the ORC system due to the regenerated 3 kW. In total, the two-phase expansion consumes slightly less heat and ends at 26.7 kW of heat transferred from an oil stream of 0.12 kg/s before the expansion. The 2 kW that are supplied to the expansion device are added to the composite curve as horizontal lines at the temperatures calculated in the last section. This heat is provided by 0.03 kg/s of thermal oil that are cooled down to 170 °C. Therefore the inclination of the two-phase expansion heat donation curve in Fig. 9 changes at that temperature and runs parallel to the other one until 200 °C are reached.

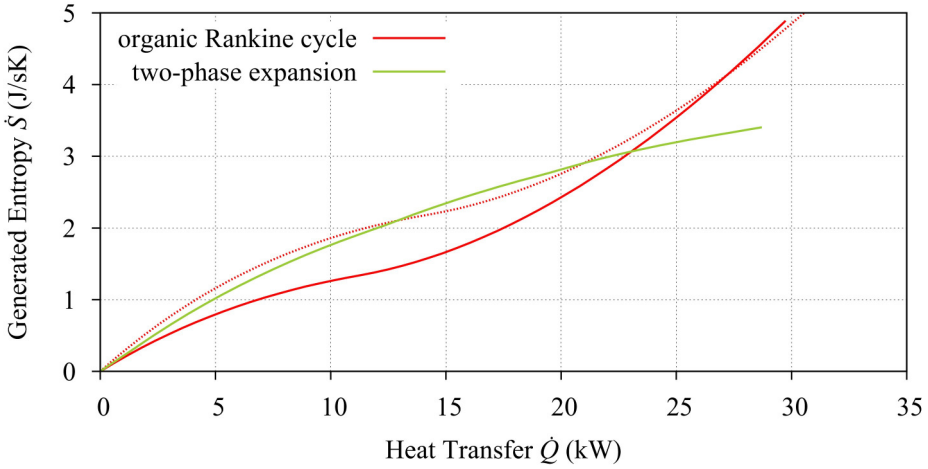

Fig. 10. Entropy generated during heat supply to organic Rankine cycle and two-phase expansion, the red dashed line depicts an organic Rankine cycle without regeneration.

Calculating the entropy generation during the heat exchange illustrates where the initial losses occur. *k* steps in terms of heat transfer are used to follow the working fluid through the heat supply. In Fig. 10, the sum of the generated entropy as given by

$$\dot{S}_{gen,j} = \sum_{i=1}^{j}\left[\left(\frac{1}{T_{mean,fluid,i}} - \frac{1}{T_{mean,src,i}}\right)\cdot\dot{Q}_i\right] \forall\ j \in \{1,\ldots,k\} \text{ with } \sum_{i=1}^{k}\dot{Q}_i = \dot{Q}_{in} \qquad (9)$$

is shown. Equation (9) combines the temperature difference between heat donating $T_{mean,src}$ and heat receiving fluid $T_{mean,fluid}$ with the amount of heat $\dot{Q}_{in}$ transferred in the regarded interval. Temperature differences cause irreversibilities. The inclination of the curves in Fig. 10 illustrates that losses occur in the beginning of the heat transfer and, in case of the ORC, also at the end while heating the alternative cycle generates less entropy at larger amounts of transferred heat.

The end points of the three lines in Fig. 10 represent the entropy generated at the end of the heat supply. It can be seen that the improvement from employing a regenerator is limited. Introducing the two-phase expansion decreases the amount of entropy generated due to heat transfer. In total, about a fourth of the entropy production can be avoided at comparable power output.

5. Simulation Results

Despite different pressure levels, results from an adapted ORC and from the steady state representation of the alternative power cycle are comparable. A more efficient heat supply in the primary heat exchanger is combined with irreversibilities from the second heat input leading to a slightly enhanced heat exchanger performance.

To compare both systems on a cycle level, different efficiencies can be calculated. Since the temperatures of the heat source T_{max} and the heat rejection fluid T_{min} are the same, both cases have an ideal efficiency $\eta_{ideal} = 1-(T_{min}/T_{max})$ of 36%. To assess the grade of the energy conversion, first law η_I and second law η_{II} efficiency are obtained from (10). Calculating the first law, or thermal, efficiency is done by comparing the net power output $\dot{W}_{net}$ to the amount of supplied thermal energy $\dot{Q}_{in}$. The first represents the surplus work after the required pump work has been subtracted from the expander output and the latter is the sum of all heat inputs to the system in primary heat exchanger and, if needed, in the expansion device. The second law efficiency of the cycle relates the output of the energy conversion to the corresponding performance of an ideal Carnot cycle η_{ideal}. Hence, the formulae used for first and second law efficiency are

$$\eta_I = \frac{\dot{W}_{net}}{\dot{Q}_{in}} \text{ and } \eta_{II} = \frac{\dot{W}_{net}}{\dot{W}_{ideal}} = \frac{\eta_I}{\eta_{ideal}}. \tag{10}$$

The net power output of all systems is around 3.1 kW, while the pump consumes more than twice the energy in the two-phase cycle. Calculating the efficiencies defined above also yields similar results of slightly more than 10% for thermal efficiency and below 30% for the second law or cycle efficiency. To investigate the potential stored in the working fluid after the heat exchange, a second ideal efficiency is defined that is solely based on the working fluid temperatures only,

$$\eta_{ideal,fluid} = 1 - \frac{T_{min,fluid}}{T_{max,fluid}}. \tag{11}$$

While ORC configurations give values between 16% and 18%, the two-phase cycle has a potential for 25%. This relates to the elevation of 40 K in maximum working fluid temperature. Considering this value, more than half of the potential work in the fluid can be converted to mechanical energy in an ORC. To obtain more information about the losses during the heat to power conversion, the exergy release of the heating fluid is calculated by solving

$$\dot{E}_{in} = \sum_{i=1}^{k} \left[\left(1 - \frac{T_0}{T_{mean,src,i}} \right) \cdot \dot{Q}_i \right] \text{ with } \sum_{i=1}^{k} \dot{Q}_i = \dot{Q}_{in}. \tag{12}$$

The temperature $T_{mean,src}$ denotes the average heating fluid temperature per segment and T_0 is the reference temperature of 25 °C.

Table 1. Performance of two-phase expansion and two organic Rankine cycles.

Parameter	*ORC, no regeneration*	*ORC, regeneration*	*Two-phase expansion*
Mass flow heat carrier (kg/s)	0.15	0.15	0.12+0.03
Mass flow working fluid (kg/s)	0.071	0.076	0.075
Total heat supply (kW)	31.1	29.7	26.7+2
Pump work (kW)	0.28	0.31	0.70
Net power out (kW)	3.1	3.1	3.1
Thermal efficiency, η_I (%)	10.0	10.6	10.8
Cycle efficiency, η_{II} (%)	27.8	29.4	29.9
Ideal efficiency, $\eta_{ideal,fluid}$ (%)	17.6	16.4	25.4
Exergy input (kW)	9.0	8.91	8.66
Exergetic efficiency, η_{ex} (%)	34.4	34.8	35.7

Considering the produced work as being only exergy, the exergetic efficiency η_{ex} is the ratio of power output and exergy input. Also by employing this technique, the alternative cycle performs close to the Rankine cycles. The advantages in terms of primary heat exchange cannot equalise the other losses that occur later in the cycle.

The performance resulting from the operation described above is summarised in Table 1 together with data for an ORC without internal heat recovery. In the column for the two-phase expansion, some rows contain two values. The second number for mass flow of oil and the amount of supplied heat express the contribution of the expansion device whereas the first value is obtained from calculations considering the primary heat exchanger.

6. Conclusion and outlook

The results from a dynamic simulation of a two-stage reciprocating device show that it is possible to design a compact expander that can extract work from working fluid supplied in liquid form. Injecting the working fluid on a fixed surface heat exchanger at simultaneous expansion with accompanying variation of the mean fluid temperature yields an increased heat transfer. This assures a minimum vapour content and minimises the risk of hydraulic locking that might occur during the precompression phase. Calculating three suitable temperatures for bulk heat addition during a step-wise expansion gives an acceptable steady state approximation of this process.

Studying the system performance including the heat supply shows that the presented system layout with the two-phase expansion performs comparable to a Rankine cycle with the same working fluid. The obtained results are sensitive to the constraints arising from the heat source definition and might change when optimising the systems for efficiency instead of power output. Furthermore, this study shows the potential benefits of enhanced heat source exploitation by utilising an unconventional expander that can operate in the two-phase regime.

Due to the number of assumption and simplifications employed in the dynamic and steady state model as well as in the overall boundary conditions, it is desirable to conduct a more detailed analysis of the proposed system. Especially flow and heat transfer calculations in the detailed expander model are sources of uncertainty. Regarding the system, several measures can be taken to generate a more comprehensive study. Among those, auxiliary power consumption and the interaction with a heat source are considered to be of major interest. Investigating the application of low temperature power cycles from a more general point of view, different working fluid should also be compared. A systematic approach on this can contribute performance gains as described by, amongst others, [12] and [13]. Including mixtures [14] and supercritical operation [15] in an efficiency assessment adds even more degrees of freedom to a future study.

Acknowledgments

The authors would like to thank their colleagues Kristian Fredslund Jensen and Nikolas Aulin Paldan at IPU for sharing their expertise regarding energy systems, experimental setups and mechanical details of the expander.

Nomenclature

Abbreviations and Acronyms

BDC bottom dead centre position of the piston

DTU Danmarks Tekniske Universitet (Technical University of Denmark)

HPC high pressure expansion chamber

LPC low pressure expansion chamber

ORC organic Rankine cycle

TDC top dead centre position of the piston

VHE Viking Heat Engines

Letter Symbols

A	area, m^2
c	coefficient
$\dot{E}$	exergy transfer rate, kW
H	enthalpy, kJ
h	specific enthalpy, kJ/kg
k	number of steps in transferred heat
$\dot{m}$	mass flow rate, kg/s
N	rotational speed, min^{-1}
p	pressure, bar
Q	heat, kJ
$\dot{Q}$	heat transfer rate, kW
Q^*	heat transferred at a certain temperature, kJ/K
$\dot{S}$	entropy rate, J/(sK)
s	specific entropy, kJ/(kgK)
T	temperature, °C
t	time, s
U	internal energy, kJ
$\dot{V}$	rate of volume change, m^3/s
$\dot{W}$	work transfer rate, kW
x	vapour content

Greek symbols

α	heat transfer coefficient, $W/(m^2 K)$
Δ	difference
η	efficiency
θ	crank angle, °
ϑ	transition coefficient
π	ratio of circumference to circle diameter
ρ	density, kg/m^3
ϕ	transition position coefficient

Subscripts and superscripts

I	first law
II	second law
0	initial value, reference
cool	cooling
d	discharge
evap	evaporation
ex	exergetic
exp	expansion
fluid	working fluid
heat	heat exchanger
ideal	ideal process

in	input
is	isentropic
max	maximum value over a defined interval
mean	average value over a defined interval
min	minimum value over a defined interval
net	net value
pump	pump
out	output, outlet
src	referring to a heat source
t	transition point
wall	cylinder wall

References

[1] International Energy Agency, Key World Energy Statistics 2011. Paris, France.

[2] Quoilin S., Lemort V., Lebrun J., Experimental study and modeling of an Organic Rankine Cycle using scroll expander. Applied Energy 2010; 87(4):1260-1268.

[3] Grill A., Springer J.-P., Aumann R., Schuster A., Spliethoff H., Simulation and experimental validation of an ORC system for waste heat recovery of exhaust gas. In: Bojić M., Lior N., Petrović J., Stefanović G., Stevanović V., editors. ECOS 2011: Proceedings of the 24th International Conference on Efficiency, Cost, Optimization, Simulation, and Environmental Impact of Energy Systems; 2011 Jul 4-7; Novi Sad, Serbia. University of Niš, Faculty of Mechanical Engineering:840-50.

[4] Daminabo F.F.O., A Novel 2kWe Biomass-Organic Rankine Cycle Micro Cogeneration System [dissertation]. Nottingham, United Kingdom: University of Nottingham; 2009.

[5] Klein S., Alvarado F.L., Engineering Equation Solver (EES) v8.874. Madison, Wisconsin, USA: F-Chart Software; 2011.

[6] Jacobsen R.T., Penoncello S.G., Lemmon E.W., Thermodynamic Properties of Cryogenic Fluids. New York, USA: Plenum Publ. Corp.; 1997.

[7] Richter C.C., Proposal of New Object-Oriented Equation-Based Model Libraries for Thermodynamic Systems [dissertation]. Braunschweig, Germany: Technical University Carolo-Wilhelmina Braunschweig; 2008.

[8] Cardoso E., Passos J., Stutz B., Lallemand M., Confined boiling of n-pentane in a horizontal space. In: EBECEM 2008, Proceedings of the 1st Brazilian Meeting of Boling, Condensation and Multiphase Liquid-Gas Flow; 2008 Apr 28–29; Florianópolis, Brazil. ACBM-UFSC:1-6.

[9] Badami M., Mura M., Preliminary design and controlling strategies of a small-scale wood waste Rankine Cycle (RC) with a reciprocating steam engine (SE). Energy 2009; 34(9):1315–1324.

[10] Saul A., Wagner, W., International Equations for the Saturation Properties of Ordinary Water Substance. Journal of Physical and Chemical Reference Data 1987; 16(4):893–901.

[11] Wagner W., Pruss A., International Equations for the Saturation Properties of Ordinary Water Substance—Revised According to the International Temperature Scale of 1990. Journal of Physical and Chemical Reference Data 1993; 22(3):783–787.

[12] Papadopoulos A.I., Stijepovic M., Linke P., On the systematic design and selection of optimal working fluids for Organic Rankine Cycles. Applied Thermal Engineering 2010; 30(6-7):760-769.

[13] Drescher U., Brüggemann D., Fluid selection for the Organic Rankine Cycle (ORC) in biomass power and heat plants. Applied Thermal Engineering 2007; 27(1):223-228.

[14] Angelino G., Colonna P., Multicomponent working fluids for organic Rankine cycles (ORCs). Energy 1998; 23(6):449–463.

[15] Schuster A., Karellas S., Aumann R., Efficiency optimization potential in supercritical Organic Rankine Cycles. Energy 2010; 35(2):1033-1039.